Journal of Materials and Environmental Science
ISSN : 2028-2508
e-ISSN : 2737-890X
CODEN : JMESCN


J. Mater. Environ. Sci., 2026, Volume 17, Issue 7, Page 1056-1067

http://www.jmaterenvironsci.com

# Performance Study of a 10 kVA Parabolic Trough Concentrated Solar Thermal Mini-Power Plant Operating with a Rankine Cycle

**Salifou CISSE [1]*, Boureima KABORE [1,2], Nebyinga Béatrice KOMI [1], Sié KAM[1]**

[1]*Laboratoire d'Energies Thermiques Renouvelables, Université Joseph KI-ZERBO, Burkina Faso.*

[2]*UFR ST, Laboratoire de Chimie Analytique, Physique spatiale et Energétique (L@CAPSE) Université Norbert ZONGO, Koudougou, Burkina Faso*

**Corresponding author, Email address: shalcisde@gmail.com*

***Received*** *26 Mar 2026,*
***Revised*** *29 June 2026,*
***Accepted*** *30 June 2026*

**Keywords:**
- ✓ *Parabolic trough collector;*
- ✓ *Concentrated solar power;*
- ✓ *Rankine cycle;*
- ✓ Decentralized electrification;
- ✓ *Burkina Faso*

***Citation****: Cisse S., Kabore B., Komi N. B., Kam S., (2026) Performance Study of a 10 kVA Parabolic Trough Concentrated Solar Thermal Mini-Power Plant Operating with a Rankine Cycle, J. Mater. Environ. Sci., 17(7), 1056-1067.*

**Abstract:** This study investigates the performance of a 10 kVA concentrated solar thermal power plant operating with a Rankine cycle, tailored to the solar irradiance conditions of Ouagadougou, Burkina Faso. The concentrating solar technology employs a solar field composed of Reflectech Plus Mirror Film modules (reflectivity 93%) to focus solar irradiation onto a SCHOTT PTR 70 receiver tube. Synthetic thermal oil transfers the thermal energy to a steam generator, which feeds a Rankine cycle using water as the working fluid. The Electratherm Green Machine twin-screw turbine (efficiency 75%) coupled with an alternator (efficiency 91%) generates a gross power of 11 kW, resulting in a net power of 10 kW after accounting for 8% auxiliary losses. The solar field efficiency reaches 33.76%, the Rankine cycle efficiency is 33.52% (compared to 37.4% for the Carnot cycle), and the overall plant efficiency is 11.32%. A molten salt-based thermal storage system enables continuous power production after sunset. Optimizations such as steam superheating or hybridization with photovoltaic systems could further enhance performance. This concentrating solar power plant has very low impacts compared to conventional energy sources. It avoids the emission of several tonnes of carbon dioxide ($CO_2$) per year while producing neither atmospheric pollutants nor radioactive waste. Thanks to the use of recyclable reflective mirrors and molten salt thermal storage, the carbon footprint over the entire life cycle remains very low.

## 1. Introduction

Global energy consumption remains dominated by fossil fuels, accounting for 81.4% of primary energy in 2015, down from 86.7% in 1973, according to the International Energy Agency (IEA, 2017), (Smil, V. 2017). This reliance leads to environmental impacts such as pollution and climate change, as well as economic consequences including rising resource costs and energy insecurity (IEA, 2023), (IPCC, 2022). Renewable energies, particularly solar energy, offer a sustainable alternative, especially in high-irradiation regions like Ouagadougou, Burkina Faso, with a global horizontal irradiance (GHI) of 471.7 W/m² and direct normal irradiance (DNI) of 364.6 W/m² (Lucas, 1980); (M. Collares Pereira *et al*.1979). Among solar technologies, concentrated solar power (CSP) systems, such as parabolic trough collectors, enable electricity generation through a thermodynamic cycle like the Rankine cycle

(Salazar *et al.* 2017); (Bellos *et al.* 2019); (Byiringo *et al.* 2025a&b). The objective of this study is to model a 10 kVA parabolic trough solar power plant to explore a new application segment for decentralized electrification. The modeling encompasses the solar field, heat transfer system, and power block. It also examines optimization prospects to improve overall efficiency, based on local irradiance data and component characteristics, thereby providing a reproducible sizing methodology scalable across the West African sub-region. This contributes to knowledge transfer and addresses energy needs in the context of the transition to clean energies (IRENA, 2023). From an environmental perspective**,** this concentrating solar power plant has very low impacts compared to conventional energy sources (Hernandez *al.*, 2014). It avoids the emission of several tonnes of carbon dioxide ($CO_2$) per year while producing neither atmospheric pollutants nor radioactive waste. Thanks to the use of recyclable reflective mirrors and molten salt thermal storage, the carbon footprint over the entire life cycle remains very low (Heath *et al.*, 2012). Installed in Ouagadougou, this facility would significantly reduce dependence on highly polluting diesel generators, which are still widely used in Burkina Faso, while promoting the development of clean, local, and sustainable energy.

## 2. Materials and Methods

### *2.1 Principle of System Operation*

The concentrated solar power (CSP) plant comprises three main components: the solar field, the heat transfer system, and the power block; thermal storage and backup are optional (Mehos et al. 2020), (IEA, 2014), (Gauché *et al.*, 2017). The solar field utilizes parabolic trough collectors equipped with Reflectech Plus Mirror Film (reflectivity 93%) to concentrate solar irradiation onto a SCHOTT PTR 70 receiver tube (Digrazia et al., 2010), (SCHOTT Solar CSP GmbH, 2013). Synthetic thermal oil, selected for its thermal stability, transfers the thermal energy to a steam generator, which supplies a Rankine cycle using water as the working fluid (Vignarooban et al., 2015). The Electratherm Green Machine twin-screw turbine (efficiency 75%) and alternator (efficiency 91%) produce a gross power of 11 kW, yielding a net power of 10 kW after 8% auxiliary losses (Ferrière, 2017). A molten salt-based thermal storage system (sodium and potassium nitrates) extends electricity production after sunset. The concentrated solar thermal power plant operates on the principle of indirect steam generation. **Figure 1** illustrates the schematic diagram of the operating principle of a concentrated solar thermal power plant.

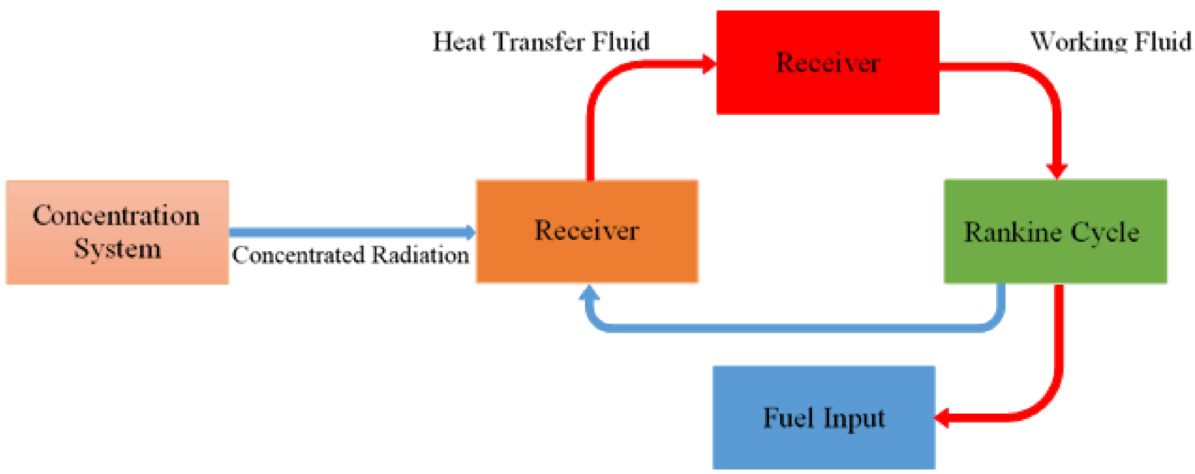


**Figure 1.** Schematic diagram of the operating principle of a concentrated solar thermal power plant

### *2.2. Modeling of System Components*

### *2.2.1. Solar Field Configuration*

The solar field configuration, consisting of four parabolic trough collectors arranged in two strings of two modules in series, optimizes land use and minimizes earthworks and leveling requirements (Collares Pereira, 1979), (Kecman *et al.*, 1969). The amount of heat absorbed by the solar field is given by **Eqn. 1** (Duffie *et al.*, 2013), (Lovegrove *et al.*, 2012) :

$$Q_{abs} = \eta_{opt}.DNI.A_T \quad \textbf{Eqn. 1}$$

Where $Q_{abs}$= useful heat captured by the collectors (W), $\eta_{opt}$= optical efficiency of the collector, $DNI$= direct normal irradiance (W/m²), $A_T$= total aperture area of the solar field (m²)
The amount of heat lost by a collector is given by **Eqn. 2** (Duffie *et al.*, 2013):

$$Q_p = U_L.A_{abs}.(T_m - T_{amb}) \quad \textbf{Eqn. 2}$$

Where $Q_p$= heat lost by a collector (W) , $U_L$= overall heat loss coefficient (W/m²·°C), $A_{abs}$= absorber surface area (m²), $T_m$= average temperature of the heat transfer fluid (°C), $T_{amb}$= ambient temperature (°C)
The amount of heat transferred to the heat transfer fluid is given by **Eqn. 3** (Chassériaux, 1984) :

$$Q_u = \dot{m}_f.C_p.(T_{out} - T_{int}) \quad \textbf{Eqn. 3}$$

Accounting for the thermal losses of the collector, we obtain:

$$Q_u = Q_{abs} - Q_p \quad \textbf{Eqn. 4}$$

Where $Q_u$= useful heat transferred to the heat transfer fluid (W), $C_p$= specific heat capacity of the fluid (J/kg·°C), $\dot{m}_f$= mass flow rate of the heat transfer fluid (kg/s), $T_{out}$,$T_{in}$= outlet and inlet temperatures of the heat transfer fluid in the absorber (°C)
The efficiency of the solar field is given by **Eqn. 5** (Duffie *et al.*, 2013) :

$$\eta_{sf} = \frac{Q_u}{A_T \times I_{incident}} \quad \textbf{Eqn. 5}$$

In terms of the optical efficiency and the heat loss coefficient, the solar field efficiency becomes:

$$\eta_{sf} = \eta_{opt} - \frac{U_L.(T_m - T_{amb})}{DNI} \quad \textbf{Eqn. 6}$$

Where $\eta_{sf}$= solar field efficiency, $DNI$ =The direct normal irradiance (W/m²)
Thermal efficiency, which represents the fraction of the solar energy absorbed by the receiver tube that is effectively transferred to the heat transfer fluid, is given by **Eqn. 7**:

$$\eta_{th} = \frac{Q_u}{Q_{abs}} \quad \textbf{Eqn. 7}$$

Where $\eta_{th}$= thermal efficiency of the receiver, $Q_u$= useful heat transferred to the heat transfer fluid (W), $Q_{abs}$= absorbed solar energy by the receiver tube (W)
In terms of thermal losses, the thermal efficiency becomes:

$$\eta_{th} = 1 - \frac{Q_p}{Q_{abs}} \quad \textbf{Eqn. 8}$$

The input parameters for the solar field include the inlet and outlet temperatures of the heat transfer fluid, direct normal irradiance, ambient temperature, and wind speed. The outputs include the mass flow rate, solar field efficiency, and absorbed energy.

### *2.2.2. Heat Transfer System*

The heat transfer in the concentrated solar thermal power plant is ensured by a network of pipes that transport the heated heat transfer fluid from the solar field to the power generation unit and return it to the solar field after cooling.

### *2.2.3. Steam Turbine*

The turbine is the key component of any steam power plant. It converts the thermal energy of the steam into mechanical rotational energy. The efficiency of a turbine is measured by comparing its power output to that of an ideal (isentropic) turbine. The efficiency of the steam turbine is given by **Eqn. 9**:

$$\eta_T = \frac{\dot{W}_{actual}}{\dot{W}_{is}} \qquad \textbf{Eqn. 9}$$

Where $\eta_T$= turbine efficiency, $\dot{W}_{actual}$= actual power output from the turbine (W), $\dot{W}_{is}$= isentropic power output of a turbine operating with the same mass flow rate and between the same two pressures (W)

Actual power is always expressed in terms of the fluid properties at the turbine inlet and outlet. It is given by **Eqn. 10** (Moran *et al.*, 2014):

$$\dot{W}_{actual} = \dot{m}(h_{in} - h_{out,actual}) \qquad \textbf{Eqn. 10}$$

Where $h_{out,actual}$ = actual specific enthalpy at the turbine outlet (J/kg)

### *2.2.4. Electric Generator*

The electric generator converts the mechanical energy from the turbine into electricity. The electrical power produced by the concentrated solar thermal power plant is given by **Eqn. 11** (Lovegrove *et al.*, 2012):

$$P_{el} = \eta_{overrall} . Q_{abs} \qquad \textbf{Eqn. 11}$$

Where $P_{el}$= electrical power generated (W), $\eta_{overrall}$= overall system efficiency, including optical, thermal, and mechanical losses.

### *2.2.5. Condenser*

The condenser condenses the steam exiting the turbine into liquid water. It rejects heat to the environment through air or water cooling. The cooling maintains a low pressure at the turbine outlet, thereby increasing the cycle efficiency.

The heat rejected by the condenser is given by **Eqn. 12** (Moran *et al.*, 2014):

$$Q_{out} = \dot{m}_{vap}(h_{vap,out} - h_{liq}) \qquad \textbf{Eqn. 12}$$

Where $Q_{out}$= rejected heat (W), $\dot{m}$ = mass flow rate of steam (kg/s), $h_{out,turbine}$= specific enthalpy of steam at the turbine outlet (J/kg), $h_{f,condensate}$= specific enthalpy of liquid water after condensation (J/kg).

### *2.2.6. Pump*

Liquid water is pumped from the condenser back to the high-pressure steam generator, closing the Rankine cycle. The pump provides the mechanical work required to increase the water pressure (Moran *et al.*, 2006). The mechanical work of the pump is given by **Eqn. 13**:

$$W_{pump} = \dot{m}_{vap} v (P_{out} - P_{in})$$ **Eqn. 13**

Where $W_{pump}$= work required by the pump (W), $v$= specific volume of water (m³/kg), $P_{out}$= outlet pressure of liquid water (Pa), $P_{in}$= inlet pressure of liquid water (Pa)

### *2.2.7. Overall Thermodynamic Efficiency of the Rankine Cycle*

The overall thermodynamic efficiency of the Rankine cycle evaluates the effectiveness of converting heat into electricity for the entire power block (Bejan, 2016). The efficiency of the Rankine cycle is given by **Eqn. 14**:

$$n_R = \frac{W_{turbine} - W_{pump}}{Q_u}$$ **Eqn. 14**

### *2.2.8. Overall System Efficiency*

The overall system efficiency, also known as sun-to-electricity efficiency, is the ratio of the net electrical power produced to the incident solar energy on the collector field (Lovegrove *et al.*, 2012). It is given by **Eqn. 15**:

$$\eta_{system} = \frac{P_{el}}{A_T \times DNI}$$ **Eqn. 15**

Where $\eta_{system}$= overall system efficiency (sun-to-electricity, $P_{el}$= net electrical power output (W), $DNI$= direct normal irradiance (W/m²)
Monthly solar irradiance data for the city of Ouagadougou, obtained from the Kamboinsé meteorological station, are presented in **Table 1**.

**Table 1**. Monthly solar irradiance values

| ***Mois*** | $GHI\ (W/m^2)$ | $DNI\ (W/m^2)$ | **Ensoleillement (kWh/m²)** |
|---|---|---|---|
| **January** | 451.8 | 441.0 | 4.52 |
| **February** | 440.6 | 356.1 | 4.41 |
| **March** | 497.7 | 330.1 | 4.90 |
| **April** | 499.8 | 353.9 | 4.98 |
| **May** | 480.9 | 288.0 | 4.97 |
| **June** | 463.8 | 304.5 | 4.74 |
| **July** | 443.1 | 283.7 | 4.59 |
| **August** | 407.7 | 238.1 | 4.40 |
| **September** | 480.7 | 304.7 | 4.51 |
| **October** | 540.5 | 581.7 | 4.70 |
| **November** | 472.0 | 452.1 | 4.65 |
| **Décember** | 481.2 | 441.0 | 4.50 |
| **Annual average** | 471.7 | 364.6 | 4.65 |

Le SCHOTT PTR 70 receiver tube minimizes thermal losses ($U_L$) at an ambient temperature of 298.15 K. The KT 800 MULTI open-type cooling tower was selected for its efficiency and low cost, featuring corrosion protection measures (plastic piping, strainers, filters). Molten salts, with a volumetric heat capacity of 2.4 J/°C·cm³, are used for thermal energy storage, with two tanks (one for cold salt at ~200 °C and one for hot salt at ~290 °C).

**Table 2.** Characteristics of the Green Machine (ElectraTherm) (Ferrière, 2007)

| Parameter | Value |
|---|---|
| **Nominal electrical power** | 10-40 kW at 350-470 V / 3 phases / 50-60 Hz |
| **Power factor** | 97 % |
| **Alternator type** | Induction |
| **Turbine type** | Twin-screw turbine |
| **Turbine efficiency** | 75 % |
| **Alternator efficiency** | 91 % |
| **Overall thermal efficiency** | >8 % |
| **Working fluid** | Water |

### *2.3. Assumptions*

- The model assumes constant clear-sky conditions with fixed maximum irradiance, which may not reflect real variations due to weather changes (e.g., clouds).
- No soiling or degradation of surfaces is considered.
- Shading and blocking losses are neglected.

## 3. Results and Discussion

### *3.1. Solar Field Performance*

**Figure 2** presents the amount of heat absorbed by the collectors, the amount of heat lost by the collectors, and the useful heat quantity. **Figure 2** shows the linear evolution of the absorbed heat flux $Q_{abs}$ and useful heat flux $Q_u$ as a function of direct normal irradiance (DNI), reaching 52.7 kW and 49.5 kW respectively at 900 W/m².

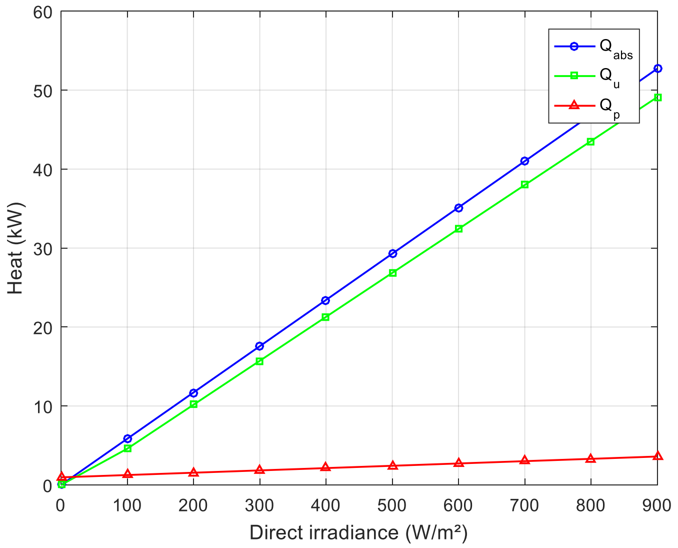


**Figure 2**. Amount of heat absorbed by the collectors, amount of heat lost by the collectors, and useful heat quantity

Thermal losses Q_loss remain very low, varying from 1.3 kW to 3.2 kW, representing less than 6% of the absorbed heat at full power. This result demonstrates excellent control of heat fluxes thanks to the use of an evacuated receiver tube with a selective coating. Although these losses increase slightly with solar irradiance (Lovegrove *et al.*, 2012), the phenomenon of convection and radiation to the environment is minimized by the SCHOTT PTR 70 receiver tube. The latter ensures high thermal performance of the parabolic trough solar field due to its very low heat loss coefficient $U_L$. **Figure 3** shows the influence of the absorber heat loss coefficient on the solar field efficiency.

**Figure 3** shows that the solar field efficiency increases with irradiance for all heat loss coefficients, rising from 0% to approximately 50–65% at 900 W/m². At high irradiance levels, the maximum efficiency (68%) is achieved with the lowest heat loss coefficient (10 W/K), while it drops to 64% for 20 W/K. Increasing this coefficient from 10 to 20 W/K results in a progressive decrease in efficiency, as thermal losses become more significant. The gap between the curves widens as irradiance increases, highlighting that a low heat loss coefficient is critical to maximize energy output under high solar irradiation (Lovegrove *et al.*, 2012); (Kennedy, 2002).

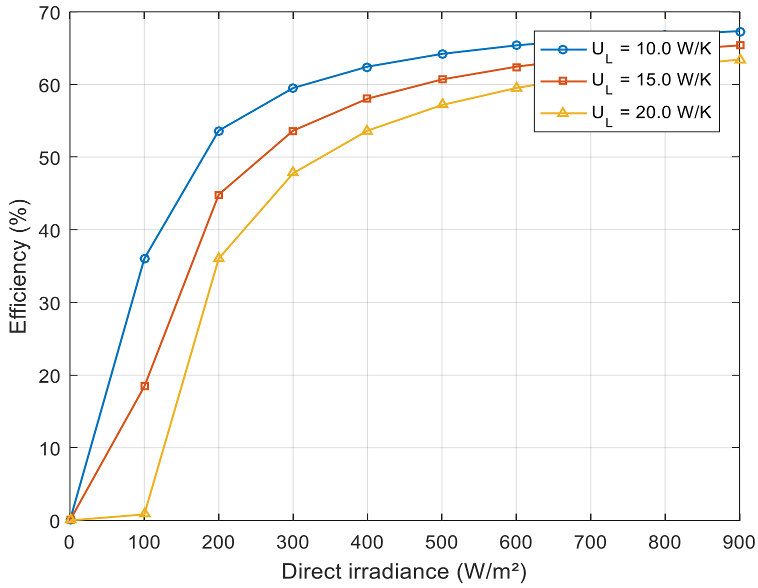


**Figure 3**. Influence of the absorber heat loss coefficient on solar field efficiency

**Figure 4** shows the influence of the collector aperture area on solar field efficiency. **Figure 4** shows that the efficiency increases with irradiance for all solar field aperture areas, rising from 0% to 68–71% at 900 W/m². The maximum efficiency (71%) is achieved with an aperture area of 150 m², decreasing to 68% for 50 m². Increasing the aperture area enables greater energy capture, resulting in a progressive improvement in efficiency across all irradiance levels (Stine *et al.*, 2001). Indeed, the efficiency depends on the absorbed heat, which is directly proportional to the solar field aperture area (Lovegrove *et al.*, 2012). Finally, this figure illustrates the electrical power generated by the system for the different direct normal irradiance values. **Figure 5** illustrates the influence of the solar field aperture area on the electrical power generated for different values of solar irradiance. **Figure 5** shows that the electrical power output increases strictly linearly with the solar field aperture area for each value of direct normal irradiance (DNI). At 900 W/m², the power rises from 6.7 $kW_e$ (for 50 m²) to 20.1 $kW_e$ (for 150 m²). The nominal power value is reached between 78 and 80 m², thereby validating the consistency of the selected sizing. Although the marginal gain slightly decreases at larger aperture areas due to increased losses (such as piping or auxiliary consumption), extending the solar field significantly boosts production while maintaining a favorable overall efficiency (Lovegrove *et al.*, 2012); (Bhutka *et al.*, 2016). These results provide an essential foundation for techno-economic optimization of small-scale parabolic trough systems.

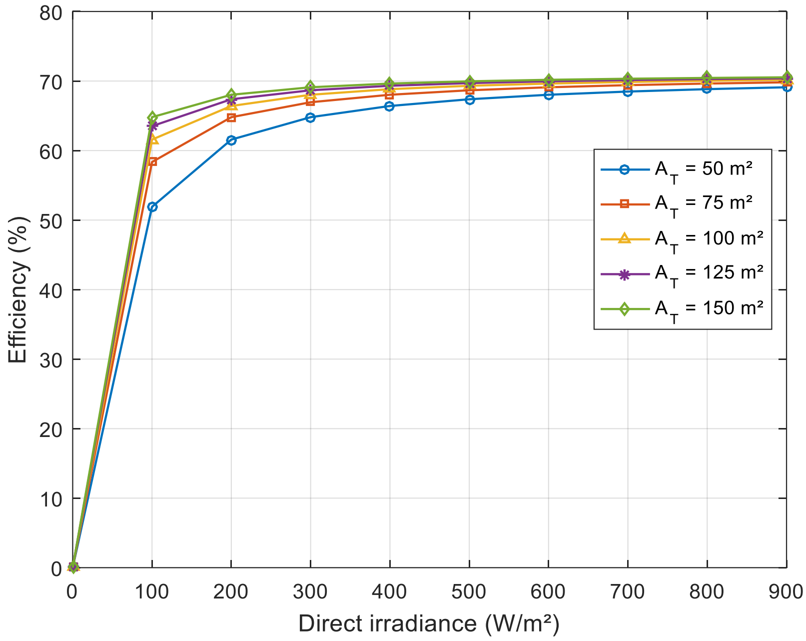


**Figure 4.** Influence of the collector aperture area on solar field efficiency

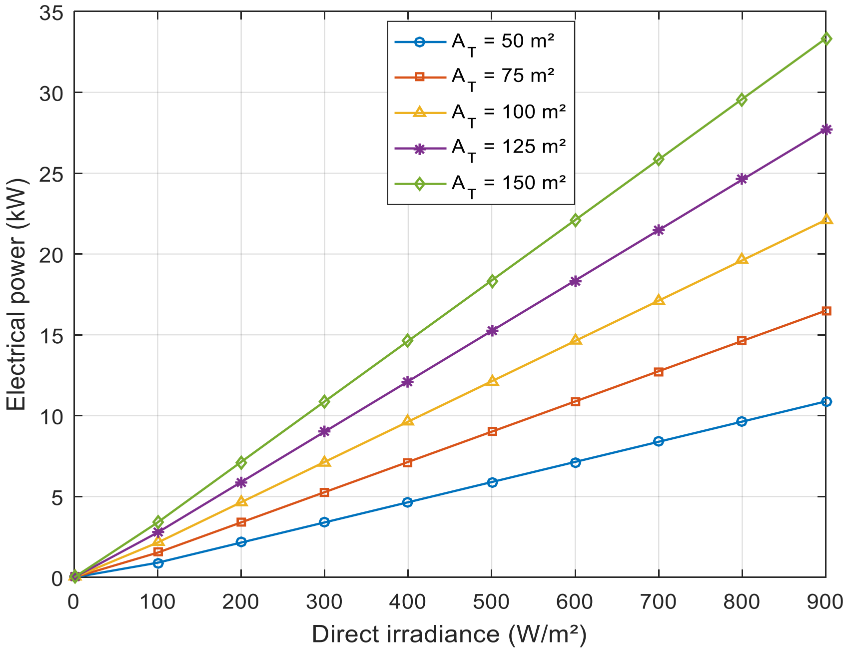


**Figure 5**. Influence of the solar field aperture area on the electrical power generated

**Figure 6** illustrates the influence of the solar field aperture area on the electrical power output over 24 hours. **Figure 6** shows that the hourly electrical power output is proportional to the solar field aperture area at a peak direct normal irradiance (DNI) of 900 W/m². At noon, the power peak increases from 11.2 kW (for 50 m²) to 17 kW (for 75 m²), with a substantial rise for larger areas: 22 kW for 100 m² and 34 kW for 150 m². However, increasing the aperture area beyond 100 m² yields only marginal gains in specific efficiency. Such an extension of the field is therefore justified primarily to increase overall energy production or to supply a more powerful turbine, highlighting an optimization plateau for the technical sizing of the system.

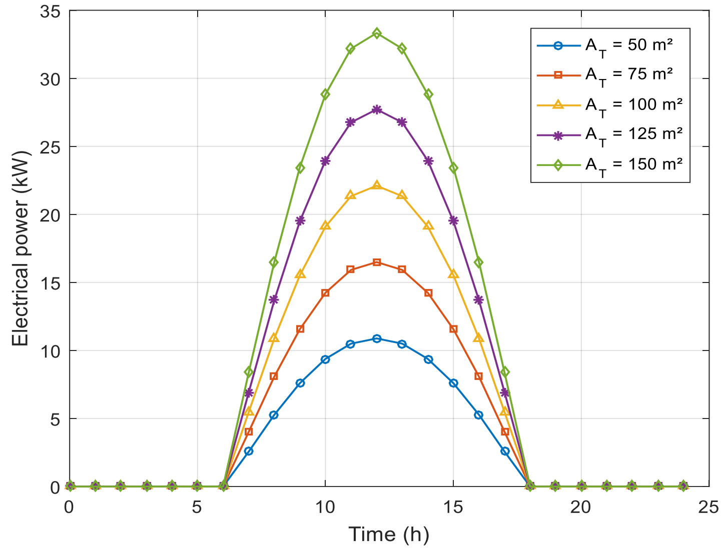


**Figure 6**. Influence of the solar field aperture area on the electrical power output over 24 hours

### *3.2. Thermal efficiency of the thermodynamic cycle*

**Figure 7** illustrates the thermal efficiency of the thermodynamic cycle as a function of temperature. **Figure 7** shows that at an operating temperature of 250 °C, the thermal efficiency is 27% for the Rankine cycle compared to a theoretical Carnot limit of 41%. At the operating temperature of 300 °C, the Rankine cycle efficiency is 30% while the Carnot efficiency is 46%. For an optimal temperature of 400 °C, the Rankine cycle thermal efficiency reaches 36% against 54% for the Carnot cycle. These results demonstrate that the thermal efficiency of the thermodynamic cycle increases with increasing operating temperature.

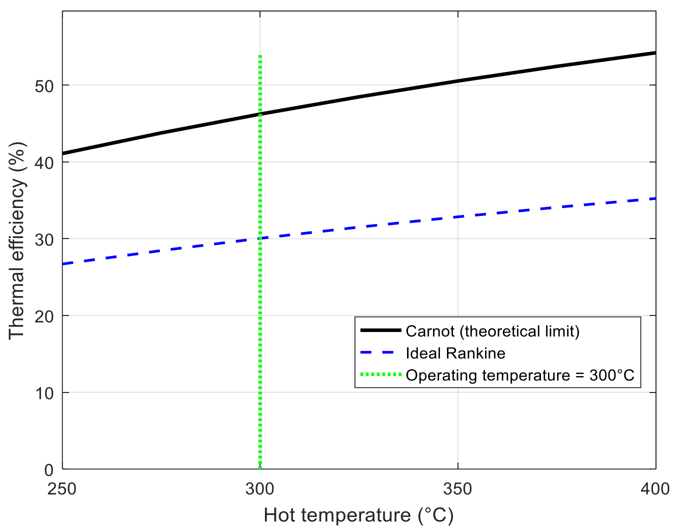


**Figure 7**. Thermal efficiency of the thermodynamic cycle as a function of temperature

### *3.3. Optimization of operating temperature*

**Figure 8** illustrates the overall system efficiency and temperature difference as a function of temperature. **Figure 8** shows that the overall efficiency is 16.8% at an operating temperature of 250 °C. When the operating temperature increases to 300 °C, the overall efficiency is 15.8%, and it rises to 20.5% at 350 °C. For the optimal temperature of 400 °C, the maximum overall system efficiency reaches 22%. This result indicates that the overall system efficiency increases with increasing operating temperature. It can be concluded that a higher operating temperature provides better system performance.

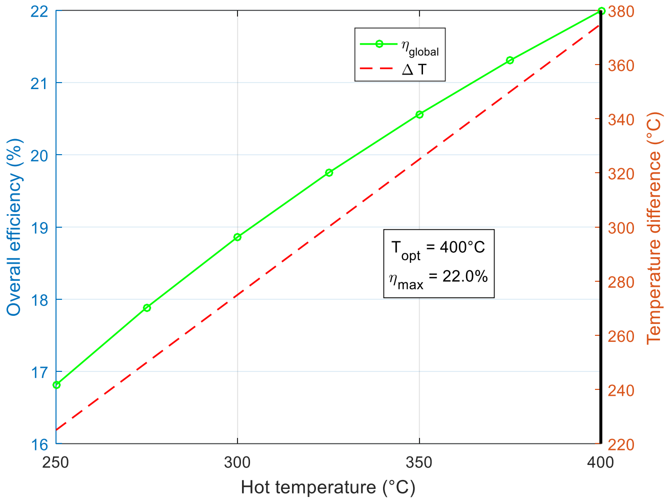


**Figure 8**. Overall system efficiency and temperature difference as a function of temperature

### *3.4. Potential Optimizations*

Several optimization prospects can be considered. Increasing the temperature of the heat transfer fluid beyond 400 °C could enhance the system efficiency but would require materials capable of withstanding high pressures. Similarly, a larger thermal storage capacity could meet prolonged energy demand. Furthermore, hybridization with photovoltaic panels could increase overall production and reduce the cost per unit of power output. Concentrated solar power (CSP) plants require significant land area, which increases investment costs. Optimization of parabolic trough collectors—such as improved optical efficiency or the use of lower-cost materials—could make the technology more accessible and economically viable for decentralized applications, as suggested by several researchers (Halimi *et al.*, 2023); (Abed *et al.*, 2024); (Chaanaoui *et al.*, 2026); (Santillon *et al.*, 2026).

## Conclusion

This study demonstrates the technical feasibility of a 10 kVA concentrated solar thermal mini-power plant optimized for the Sahelian context, particularly in Ouagadougou, Burkina Faso. The use of high-performance components, such as Reflectech Plus Mirror Film (93% reflectivity) and the SCHOTT PTR 70 evacuated receiver tube, enables excellent thermal flux management with losses limited to less than 6%. The analyses show that the thermal-to-electrical efficiency stabilizes at a remarkable 24% for DNI values above 600 W/m², proving the system's effectiveness even under moderate irradiance conditions. The solar field aperture area, ideally sized between 78 and 100 m², ensures a nominal electrical output of 10 kW while minimizing investment costs. The integration of a molten salt thermal storage system represents a major advantage, increasing the daily capacity factor from 22% (without storage) to 55% (with storage). This technology guarantees more than 17 hours of continuous operation, delivering stable power of 16.2 $kW_e$ after sunset to meet nighttime peak demand. Furthermore, the study highlights that raising the operating temperature toward 400 °C could achieve a maximum overall system efficiency of 22%. These results confirm that small-scale CSP plants with thermal storage offer a dispatchable and economically relevant solution for decentralized electrification in West Africa. Future optimizations, such as photovoltaic hybridization or steam superheating, could further enhance performance. In conclusion, this model provides a reproducible sizing methodology that supports the transition to clean energy in the sub-region.

**Disclosure statement**: *Conflict of Interest*: The authors declare that there are no conflicts of interest. *Compliance with Ethical Standards*: This article does not contain any studies involving human or animal subjects.

## References


Abed, A.A., El-Marghany M.R., El-Awady, W.M., Hamed, A.M. (2024). Recent advances in parabolic dish solar concentrators: Receiver design, heat loss reduction, and nanofluid optimization for enhanced efficiency and applications, *Solar Energy Materials and Solar Cells*, 273, 112930, ISSN 0927-0248, https://doi.org/10.1016/j.solmat.2024.112930

Bejan, A. (2016). *Advanced Engineering Thermodynamics*. John Wiley & Sons.

Bellos, E., & Tzivanidis, C. (2019). Alternative designs of parabolic trough solar collectors. *Progress in Energy and Combustion Science*, 71, 81-117. https://doi.org/10.1016/j.pecs.2018.11.001

Bhutka, J., Gajjar, J. and Harinarayana, T. (2016). Modelling of Solar Thermal Power Plant Using Parabolic Trough Collector. *Journal of Power and Energy Engineering*, 4, 9-25. http://dx.doi.org/10.4236/jpee.2016.48002

Byiringiro, J., Chaanaoui, M., Hammouti, B. (2025). Thermal performance enhancement of a novel receiver for parabolic trough solar collector. *Interactions*, 246, 13 https://doi.org/10.1007/s10751-024-02230-3

Byiringiro, J., Chaanaoui M., Hammouti B. (2025) Enhancement of thermal performance in parabolic trough solar Collectors: Investigation of three novel receiver configurations using advanced heat transfer fluids, *Solar Energy Materials and Solar Cell*, 293, 113833, https://doi.org/10.1016/j.solmat.2025.113833

Chaanaoui, M., Byiringiro, J. & Hammouti, B. (2026) Cost modeling of innovative metal 3D printed solar absorber tubes for high-efficiency parabolic trough collector. *Int J Adv Manuf Technol.* 142, 3835–3849, https://doi.org/10.1007/s00170-025-17286-w

Chassériaux, J. M. (1984). *Conversion thermique du rayonnement solaire*. Paris : Dunod.

Collares Pereira M. et A. Rabi (1979). The Average Distribution of Solar Radiation, *Solar Energy*, Vol. 22, pp. 155–164.

Digrazia M., R. Gee, and G. Jorgensen (2009). “ReflecTech® Mirror Film Attributes and Durability for CSP Applications”, *ASME Conference, Sustainability 2009*.

Duffie, J.A. and Beckman, W.A. (2013). *Solar Engineering of Thermal Processes*. 2nd Edition, John Wiley & Sons, Hoboken. https://doi.org/10.1002/9781118671603

Ferrière A. (2007). *Les technologies solaires à concentration appliquées à la production d’électricité et d’hydrogène*, séminaire IPN Orsay.

Gauché, P., et al. (2017). System value and progress of CSP. *Solar Energy*, 152, 106-139.

IEA (International Energy Agency) (2014). *Technology Roadmap: Solar Thermal Electricity*. Paris: OECD/IEA.

Halimi, M., El Amrani A., Chaanaoui, M., Amrani A., Oumachtaq, A., Messaoudi C. (2023). Investigation of parabolic trough collector receiver with U-pipe exchanger using a numerical approach: Towards temperature non-uniformity optimization, *Applied Thermal Engineering*, 234, 121335, ISSN 1359-4311, https://doi.org/10.1016/j.applthermaleng.2023.121335.

Heath, G. A., et al. (2012). *Life Cycle Greenhouse Gas Emissions from Concentrating Solar Power*. National Renewable Energy Laboratory (NREL), NREL/FS-6A20-56416.

Hernandez, R. R., et al. (2014). Environmental impacts of utility-scale solar energy. *Renewable and Sustainable Energy Reviews*, 29, 766-779. https://doi.org/10.1016/j.rser.2013.08.041

IEA (2017). *Key World Energy Statistics 2017*. International Energy Agency, Paris.

IEA (International Energy Agency) (2023). *World Energy Outlook 2023*. Paris: OECD/IEA.
IPCC (2022). *Climate Change 2022: Mitigation of Climate Change*. Cambridge University Press.
IRENA (2023). *Renewable Energy Market Analysis: Africa and its Regions*. International Renewable Energy Agency.
Kecman J.H. et al. (1969). *Steam Tables*, Wiley, New York.
Kennedy, C. E. (2002). *Review of Mid- to High-Temperature Solar Selective Absorber Materials*. NREL/TP-520-31267.
Lovegrove, K. and Stein, W. (2012). *Concentrating Solar Power Technology*. Woodhead Publishing, Cambridge. https://doi.org/10.1533/9780857096173
Lucas L. (1980). *Le guide des énergies douces*, Dargaud Editeur.
Matteo, Laura, et Nicolas Tauveron (2024). Générer de la vapeur pour produire de l'électricité dans les centrales nucléaires. *Comptes Rendus. Mécanique* 352(S1), 35–41. https://doi.org/10.5802/crmeca.260
Mehos, Mark, et al. (2020). *Concentrating Solar Power Best Practices Study*. Golden, CO: NREL. https://www.nrel.gov/docs/fy20osti/75763.pdf
Moran, M.J. and Shapiro, H.N. (2006). *Fundamentals of Engineering Thermodynamics*. 5th Edition, John Wiley & Sons, Inc.
Moran, M. J., Shapiro, H. N., Boettner, D. D., & Bailey, M. B. (2014). *Fundamentals of Engineering Thermodynamics*. John Wiley & Sons.
Pelay, U., et al. (2017). Thermal energy storage systems for concentrating solar power plants. *Renewable and Sustainable Energy Reviews*.
Salazar, Germán A., et al. (2017). "Analytic modeling of parabolic trough solar thermal power plants," *Energy*, vol. 138(C). DOI: 10.1016/j.energy.2017.07.110
Santillan Gomez H., Gosgot Angeles W., Yalta Chappa M., Espinoza Canaza F.I., Delgado Rodríguez Y., Oliva Cruz M., Gamarra Torres O., Barrena Gurbillón M.Á. (2026). Experimental Evaluation of the Parabolic Trough Solar Collector Under Cloudy Conditions: Case Study in Chachapoyas, *Peru. Solar*. 6(2), 17. https://doi.org/10.3390/solar6020017
SCHOTT Solar CSP GmbH. (2013). *SCHOTT PTR®70 Receiver - Technical Data Sheet*.
Sioshansi, R. and Denholm, P. (2010). The Value of Concentrating Solar Power and Thermal Energy Storage. *IEEE Transactions on Sustainable Energy*, 1, 173-183. https://doi.org/10.1109/TSTE.2010.2052078
Smil, V. (2017). *Energy Transitions: Global and National Perspectives*. Praeger.
Stine, W. B., & Geyer, M. (2001). *Power From the Sun*.
Vignarooban, K., et al. (2015). Heat transfer fluids for concentrating solar power systems – A review. *Applied Energy*.

(2026) ; http://www.jmaterenvironsci.com